# The application of orthogonal photolithography to micro-scale organic field effect transistors and complementary inverters on flexible substrate

Jingon Jang,[1] Younggul Song,[1] Hyuntaek Oh,[2] Daekyoung Yoo,[1] Dongku Kim,[1] Hyungwoo Lee,[1] Seunghun Hong,[1] Jin-Kyun Lee,[2,a)] and Takhee Lee[1,b)]
[1]*Department of Physics and Astronomy, and Institute of Applied Physics, Seoul National University, Seoul 151-747, South Korea*
[2]*Department of Polymer Science and Engineering, Inha University, Incheon 402-751, South Korea*

(Received 6 November 2013; accepted 15 January 2014; published online 3 February 2014)

Micro-scale pentacene organic field effect transistors (OFETs) were fabricated on a flexible poly(ethylene terephthalate) (PET) substrate. By applying a highly fluorinated developing solvents and its compatible photoresist materials, it has become possible to make the micro-scale patterning for organic devices using standard photolithography without damaging the underlying polymer layers. The flexible pentacene OFETs with 3 $\mu$m-sized channel length exhibited stable electrical characteristics under bent configurations and under a large number of repetitive bending cycles. Furthermore, we demonstrated micro-scale organic complementary inverters on a flexible PET substrate using p-type pentacene and n-type copper hexadecafluorophthalocyanine materials. © *2014 AIP Publishing LLC*. [http://dx.doi.org/10.1063/1.4863678]

Organic electronic devices have generated a great deal of research interest in recent years because of their outstanding advantages compared to inorganic counterparts, such as simple device architecture, low manufacturing cost, ease of fabrication, large area processing capabilities, limitless material variety, and a wide span of potential applications, including organic field effect transistors (OFETs), photovoltaic cells, memories, light-emitting diodes, and sensors.[1–7] Furthermore, the mechanical elasticity and solution processability of organic materials is a desirable feature for future flexible electronics.[8–11] From the manufacturing point of view, the material diversity and excellent solubility in common organic solvents of organic materials has made it possible to apply various device fabrication methods to organic electronics, such as shadow mask evaporation, spin-coating, ink-jet printing, and roll-to-roll printing.[12–17] However, it is still difficult to apply a standard photolithographic patterning technique to organic electronics even though this technique is the simplest way to achieve the micro-scale patterning and has already been fully optimized for the inorganic electronic devices. This cumbersome situation results mainly from a chemical incompatibility existing in organic electronic materials and organic solvents for photolithographic processing. Organic solvents are used to deposit and erase photoresist layers, but the problem is the lack of selectivity in dissolving only the photoresist not the organic electronic materials. To settle down this problem, the chemically non-damaging orthogonal photolithographic method has been introduced based on the notion of miscibility and orthogonality among materials. Miscibility allows the removal of the unnecessary part of the deposited photoresist layer by the developing solvents, and orthogonality is required to protect the underlying polymer films from the addition of lithographic chemicals.[18] Because the vast majority of organic materials, regardless of their polarity, generally show their orthogonal properties to highly fluorinated chemicals, the fluorous solvents have been recognized as a strong candidate recently for photolithographic processing of organic electronic materials. Among the various fluorous solvents, segregated hydrofluoroethers (HFEs) have been selected due to their outstanding properties, such as nonflammability, zero ozone-depletion potential, and very low toxicity for humans.[19] Studies related to the orthogonal processing of organic electronic devices using semi-perfluoroalkyl resorcinarene, which is processable in HFEs, have been reported on solid substrates.[18–20] However, its application for flexible organic devices has never been demonstrated so far.

In this study, we fabricated micro-scale OFET devices and complementary inverters on a flexible poly(ethylene terephthalate) (PET) substrate by orthogonal photolithography using HFE developing solvents and its comparable semi-perfluoroalkyl resorcinarene photoresist. We characterized the electrical properties of the fabricated micro-scale OFET devices under both flat and various bending conditions, such as different bending radius configurations and repeated bending cycles. Moreover, our micro-scale organic complementary inverters show the stable logic inverter operation as voltage transfer characteristics.

Fig. 1(a) shows the device fabrication process of the OFET devices in our study. To fabricate the devices, the PET substrate was first cleaned by a standard solvent-cleaning process using de-ionized (DI) water, acetone, and 2-propyl-alcohol (IPA) in an ultrasonic bath for 5 min at each cleaning. Next, the PET substrate was dried at 100 °C for 1 h in a vacuum oven to evaporate the residual solvent and moisture. The bottom gate Al electrodes of 30 nm thickness were deposited by a thermal evaporator using a shadow mask with a deposition rate of 0.5 Å/s at a pressure of $\sim 10^{-6}$ Torr. After the substrate was cooled, the bottom gate Al gate electrodes/PET substrate were exposed to UV-ozone treatment for 10 min to improve the film uniformity.[21] To fabricate the polymer dielectric layer,

a)E-mail address: jkl36@inha.ac.kr
b)E-mail address: tlee@snu.ac.kr

 

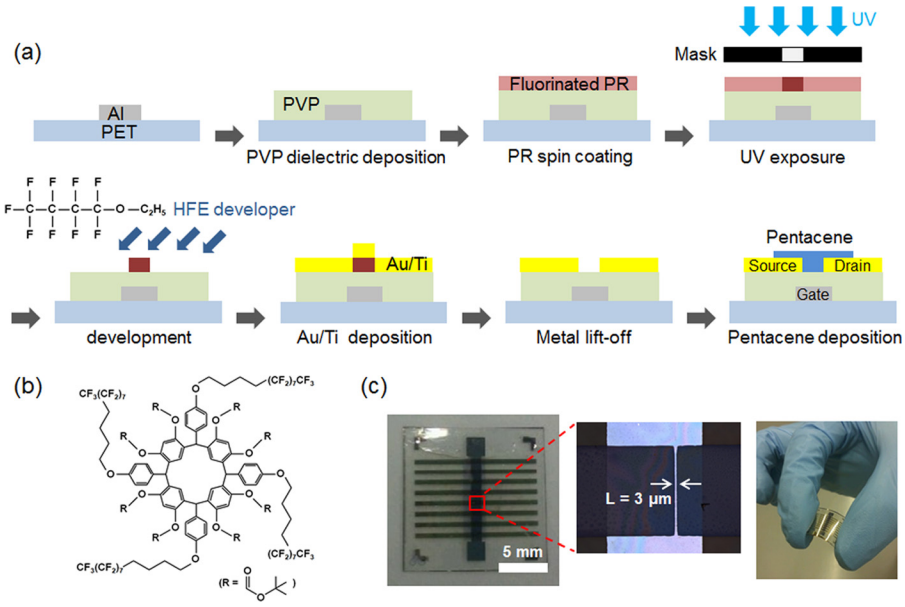


FIG. 1. (a) The device fabrication processes of the flexible pentacene OFET devices. The molecular formula in the development process shows the orthogonal developer of HFE 7200. (b) The molecular structure of semi-perfluoroalkyl resorcinarene photoresist. (c) Photographic and optical microscopic images of our flexible pentacene OFET devices.

15 wt. % of poly(4-vinylphenol) (PVP) and 3 wt. % of poly(melamine-co-formaldehyde) as a cross-linking agent were dissolved in a solvent of propylene glycol methyl ether acetate (PGMEA) without further purification. The mixed PVP solution was spin-coated onto the Al gate electrodes/PET substrate at 3000 rpm for 30 s, followed by soft-baking on a hotplate at 100 °C for 10 min in a $N_2$-filled glove box. After the PVP film on the Al pad was removed with a methanol-soaked swab for electrical probing, the PVP film was hard-baked on a hotplate at 200 °C for 1 h.[22] The deposited PVP film thickness was measured at ~1 $\mu$m using an Alpha-step profiler. To prepare the fluorinated photoresist solution, 15 wt. % of the previously reported semi-perfluoroalkyl resorcinarene (Fig. 1(b)) powder and 0.5 wt. % of N-nonafluorobutanesulfonyloxy-1,8-naphthalimide photoacid generator were dissolved in a mixed solvent (3-ethoxy-1,1,2,3,4,4,5,5,6,6,6-dodecafluoro-2-trifluoromethylhexane (HFE 7500 purchased from 3M): PGMEA = 4:1 weight ratio) and the solution was filtered through a 0.20 $\mu$m-sized nylon syringe filter.[19] Then, the fluorinated photoresist solution was spin-coated at 1500 rpm for 60 s and baked on a hotplate at 75 °C for 3 min in a clean room under yellow light. Subsequently, the coated photoresist film was exposed under UV light (416 nm wavelength, intensity of ~10 mW/cm$^2$) through a chromium-patterned photomask by a mask aligner. After an additional baking process at 75 °C for 3 min, the unexposed photoresist below the chromium-drawn region in the photomask was cleaned off by a developing solvent of ethoxy-nonafluorobutane (HFE 7200) and dried with $N_2$ gas. Because our fluorinated photoresist leaves negative-tone images, UV-exposed regions undergo chemical reactions losing solubility in the fluorous developing solvent, whereas unexposed parts can be washed away by the same developer enabling micro-patterning process without damaging the PVP dielectric layer. To fabricate the source/drain electrodes, 30 nm-thick Au was deposited after the deposition of a 5 nm-thick Ti adhesion layer on the developed samples by an electron beam evaporator with a deposition rate of 0.5 Å/s at a pressure of ~$10^{-7}$ Torr. After the metal lift-off process using a lift-off solvent (HFE7200: ethanol = 20:1 weight ratio), the 3 $\mu$m-sized micro-gap between the source/drain electrodes became the active channel length of our OFET devices (Fig. 1(c)). Finally, the pentacene active film with 60 nm thickness was deposited by a thermal evaporator with a deposition rate of 0.5 Å/s at a pressure of ~$10^{-6}$ Torr. In case of the complementary inverter devices, additional thermal evaporation process of n-type copper hexadecafluorophthalocyanine ($F_{16}$CuPc) material was done at the same deposition rate and pressure conditions as the p-type pentacene deposition on opposite region of pentacene film sharing output voltage line using a shadow mask. Fig. 1(c) shows photographic and optical microscopic images of the completely fabricated OFET devices.

The electrical data of the fabricated OFET devices were measured using a Keithley 4200-SCS parameter analyzer connected to a probe station inside an $N_2$-filled glove box. The electrical characteristics of micro-scale pentacene OFET devices are summarized in Fig. 2. All data in this figure were measured from the devices on the PET substrate under flat conditions. Fig. 2(a) shows the transfer characteristics (drain current versus gate voltage) for a fixed drain-source voltage of −40 V in the semi-logarithmic scale. It showed typical p-type transfer characteristics using the pentacene active channel layer. The current on/off ratio was observed somewhat low as $10^2$–$10^3$ due to the presence of injection barrier and short channel geometry.[23,24] Because the series resistance usually decreases as the channel length decreases, the drain current of the device with a 3 $\mu$m-channel length exhibited a higher current value than the longer-channel devices. Fig. 2(b) shows the output characteristics (drain current versus drain voltage) for different gate voltages for the 3 $\mu$m-channel device. The output characteristics exhibited a non-linear curve in a low voltage region, suggesting the presence of an injection barrier at metal/pentacene contacts. This injection contact barrier generally comes from the band offset between work function of Au electrodes (~5.0 eV) and highest occupied molecular orbital level (~5.2 eV) of pentacene active layer with formation of interfacial dipoles.

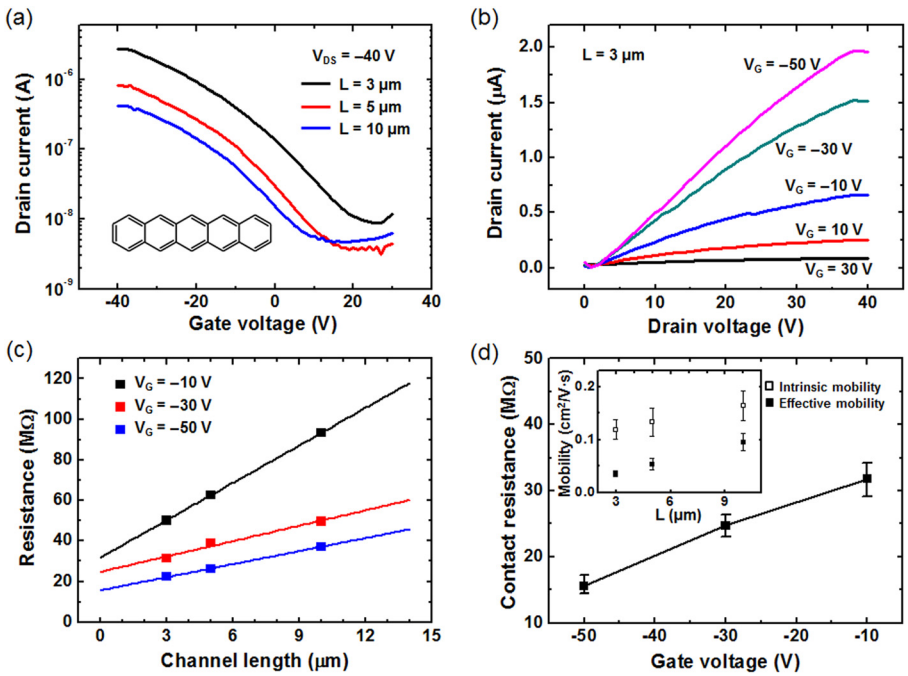


FIG. 2. (a) Transfer characteristics for the pentacene OFET devices with various channel lengths of 3, 5, and 10 $\mu$m, respectively, at a fixed gate voltage of −40 V. The molecular structure of pentacene is shown. (b) Output characteristics for the devices with a 3 $\mu$m-channel length. (c) Series resistance versus channel length at gate voltages of −10, −30, and −50 V. (d) Contact resistance obtained in (c) at gate voltages of −10, −30, and −50 V. The inset shows the field effect mobility data for devices with different channel length (L) of 3, 5, and 10 $\mu$m.

Because this contact barrier hinders the charge transport from Au electrode to pentacene layer at low voltage region showing the non-linear I-V characteristics, many researches to overcome this effect has been done such as inserting interlayer, contact-area-limited doping, and changing the electrode by graphene films or carbon nanotubes.[25–28] Nevertheless, the resistance values were approximately obtained from the slopes of the linear segments in the proper non-zero drain voltage linear region (around 5 V) of the output curve in Fig. 2(b) and plotted as a function of the channel length, as shown in Fig. 2(c). The resistance decreased as the channel length decreased due to the aforementioned dependence of the series resistance on the channel length. Likewise, the resistance decreased as the gate voltage increased in the negative gate voltage direction because the drain current of the majority hole carriers in the p-type OFET devices rapidly increased to the ON current with increased gate voltage to the negative voltage direction as shown in the transfer curve in Fig. 2(a). The contact resistance value can also be obtained as the y-intercept of the linear fitting line of the discrete resistance data versus channel length.[29–31] Fig. 2(d) displays the contact resistance as a function of the gate voltage, showing that the contact resistance decreased as the gate voltage increased to the negative direction. This result can be explained as follows: When a large negative gate voltage is applied to short channel p-type devices, high carrier density in the conducting channel region can cause a small voltage drop over the contact region and as such an accumulation of carriers narrows the width of contact barrier.[32,33] For this reason, the higher negative gate voltage reduces the contact resistance (Fig. 2(d)) as well as the series resistance (Fig. 2(c)) of our OFET devices. Here, the contact resistance for the gate voltage of −50 V was determined to be ∼15 MΩ, which is not a negligible value compared with the total resistance values of approximately 20–40 MΩ for various channels of devices (Fig. 2(c)). The inset of Fig. 2(d) shows the field effect mobility data of the OFET devices. Our devices showed a typical value of effective mobility of 0.04 to 0.1 $cm^2/V \cdot s$ for different channel lengths (L) of 3, 5, and 10 $\mu$m (filled squares), respectively. Because the contact resistance effect in our OFET devices is not negligible, it is needed to find out the mobility of the channel-effect itself (intrinsic mobility) which is related to charge carrier transport in the channel without taking into account the contact resistance. By using the corrected contact resistance extraction method, we obtained the intrinsic mobility values and plotted them in the inset of Fig. 2(d) (open squares).[32,34] The intrinsic mobility was determined to be 0.1 to 0.2 $cm^2/V \cdot s$ for our pentacene OFET devices, which is comparable to the typical intrinsic mobility values of the pentacene OFETs as stated elsewhere.[35]

We also characterized our pentacene OFET devices under different bending conditions in order to examine the stability and reliability in flexible situations. Fig. 3(a) shows the photos of the experimental setup for electrical measurement under bending conditions in $N_2$-filled glove box. The electrical parameters (ON current, mobility, and threshold voltage) of flexible pentacene OFET devices in flat (radius of ∞) and bending conditions (radius of 20 mm and 10 mm) are shown in Figs. 3(b)–3(d). The term, mobility, here denotes the effective mobility. It can be seen that each of these electrical parameters were stably maintained without any substantial fluctuation under different bending conditions (for instance, ON current of ∼2 $\mu$A, mobility of ∼0.04 $cm^2/V \cdot s$, and threshold voltage of ∼10 V for the 3 $\mu$m-channel devices). The error bars in all these figures were obtained from measuring the standard deviation of about five devices for each data point. For the possibility of practical application of flexible organic devices, it is essential to show the device reliability with repeated bending stress.[36,37] Therefore, we investigated the electrical parameters after the repeated bending cycles as summarized in inset of Fig. 4(a). One bending number denotes one cycle from the flat condition to the bending condition (radius of 10 mm) and

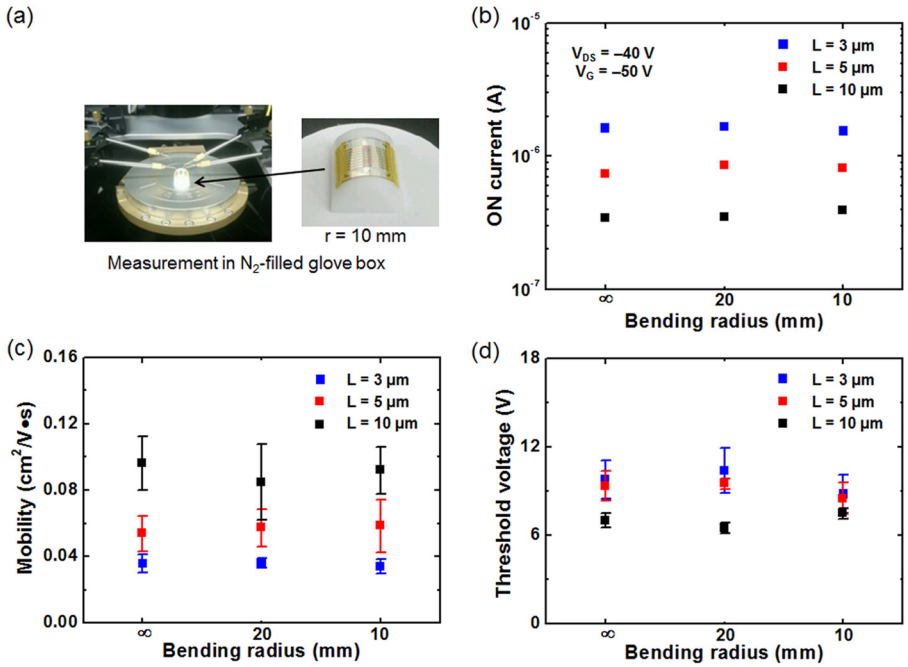


FIG. 3. (a) Photographic image of electrical measurement process for our flexible OFET devices in $N_2$-filled glove box system. (b)–(d) The electrical parameters (ON current, mobility, and threshold voltage) of our flexible OFET devices with different channel length under bent configurations.

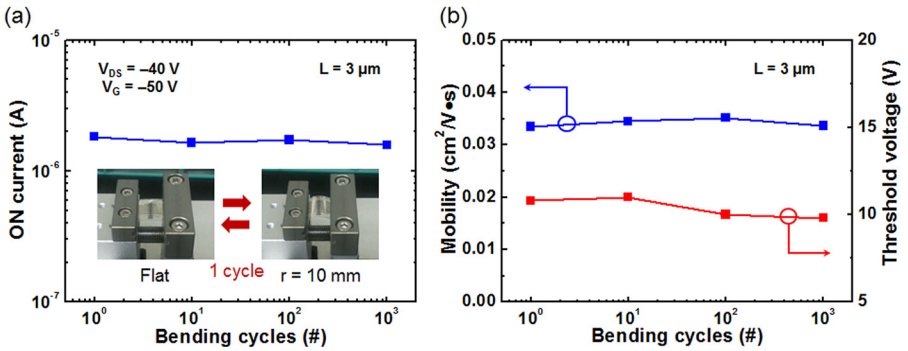


FIG. 4. The electrical parameters of (a) ON current and (b) mobility and threshold voltage for our flexible OFET devices after repeated bending cycles. The photographic images in (a) show the device under bending cycling measurement.

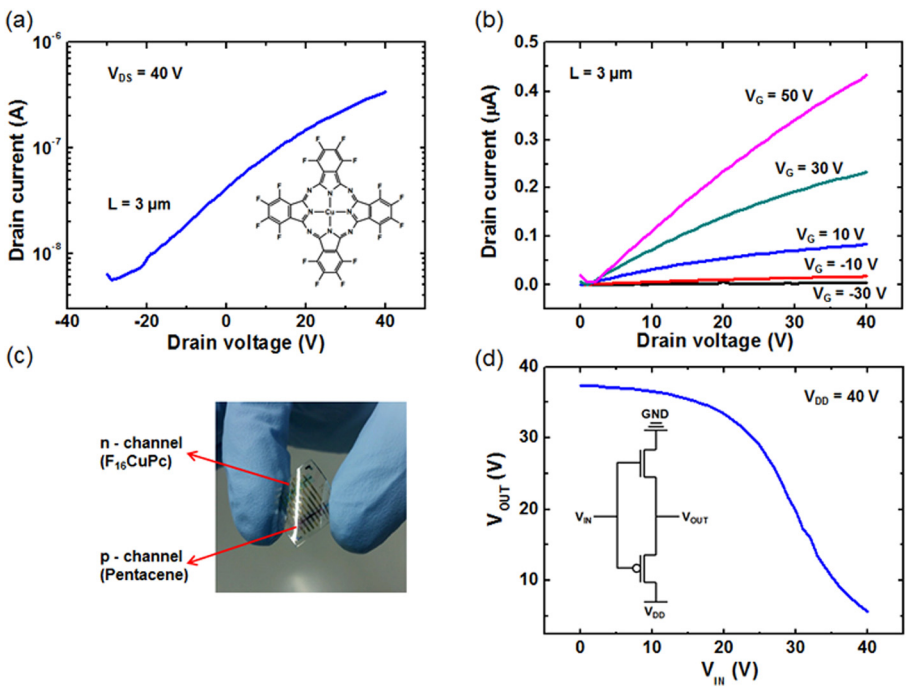


FIG. 5. (a) Transfer and (b) output characteristics for the $F_{16}$CuPc OFET devices with a 3 $\mu$m-channel length. The molecular structure of $F_{16}$CuPc is shown. (c) Photographic image of complementary inverter devices composed of p-type pentacene and n-type $F_{16}$CuPc channel layers. (d) The voltage transfer characteristics of a flexible complementary inverter at $V_{DD} = 40$ V. The inset shows the circuit configuration of the complementary inverter.

back to the flat. An automatic bending machine (inset images of Fig. 4(a)) counted the bending cycle number. From Fig. 4, one can see that the electrical parameters (ON current, mobility, and threshold voltage) were well maintained over the bending cycles up to $10^3$ times without any serious degradation.

In addition to fabrication of micro-scale single OFET devices, it has naturally become possible to fabricate the complementary inverters by linking two opposite type micro-scale single OFETs (p-type pentacene OFET and n-type $F_{16}$CuPc OFET). $F_{16}$CuPc is well known to be a stable n-type semiconductor material with excellent electrical and mechanical properties and generally used as n-type active channel layer in organic complementary logic circuit with p-type pentacene material.[38,39] Because $F_{16}$CuPc has very similar lowest unoccupied molecular orbital level (~4.8 eV) to work function of Au (~5.0 eV), it is suitable to be n-channel layer in our complementary inverters with Au source/drain electrodes.[40] The transfer electrical characteristics of micro-scale $F_{16}$CuPc OFET devices are shown in Fig. 5(a) with the molecular formula of $F_{16}$CuPc material, and output characteristics of that is also shown in Fig. 5(b). The complementary inverter consists common bottom gate line ($V_{IN}$), p-type pentacene OFET, n-type $F_{16}$CuPc OFET, and shared output voltage line ($V_{OUT}$) as shown in Fig. 5(c). Its circuit configuration is drawn in inset of Fig. 5(d). Owing to the compatibility between pentacene and $F_{16}$CuPc OFET in transfer properties, our micro-scale organic complementary inverters showed the stable logic inverter operation as voltage transfer characteristics at $V_{DD} = 40$ V (Fig. 5(d)).

In summary, we fabricated micro-scale OFET devices and complementary inverters on flexible substrates by a conventional photolithography manufacturing process using a highly fluorinated developing solvent and its comparable photoresist. This technique has made it possible to form lithographic patterning for organic devices without damaging the underlying polymer films based on the principle of orthogonality of materials. The fabricated, 3 $\mu$m-channel pentacene OFET devices showed stable electrical characteristics in both flat and bending conditions and also exhibited electrical reliability even with repeated bending cycles of up to $10^3$ times. Moreover, our flexible micro-scale organic complementary inverters composed of p-type pentacene and n-type $F_{16}$CuPc OFET devices showed the stable logic inverter operation as voltage transfer characteristics.

The authors acknowledge the financial support from the National Creative Research Laboratory program (Grant No. 2012026372) and the National Core Research Center (Grant No. 2008-0062606) through the National Research Foundation of Korea (NRF) funded by the Korean Ministry of Science, ICT & Future Planning. S.H. acknowledges the support from the NRF grant (No. 2009-0079103) and J.-K.L. thanks the financial support from the Fundamental R&D Program for Core Technology of Materials (grant # 10041220) funded by the Korean Ministry of Knowledge Economy.

[1]H. Klauk, *Organic Electronics 2: More Materials and Applications* (Wiley-VCH Verlag & Co. KGaA, Weinheim, 2012).
[2]M. Iwamoto, Y.-S. Kwon, and T. Lee, *Nanoscale Interface for Organic Electronics* (World Scientific, Singapore, 2010).
[3]G. Li, R. Zhu, and Y. Yang, Nat. Photon. **6**, 153 (2012).
[4]B. Cho, S. Song, Y. Ji, T.-W. Kim, and T. Lee, Adv. Funct. Mater. **21**, 2806 (2011).
[5]C. W. Tang and S. A. VanSlyke, Appl. Phys. Lett. **51**, 913 (1987).
[6]K.-J. Baeg, M. Binda, D. Natali, M. Caironi, and Y.-Y. Noh, Adv. Mater. **25**, 4267 (2013).
[7]W. Cheng, Z. Wu, S. Wen, B. Xu, H. Li, F. Zhu, and W. Tian, Org. Electron. **14**, 2124 (2013).
[8]M. Kaltenbrunner, T. Sekitani, J. Reeder, T. Yokota, K. Kuribara, T. Tokuhara, M. Drack, R. Schwodiauer, I. Graz, S. Bauer-Gogonea, S. Bauer, and T. Someya, Nature **499**, 458 (2013).
[9]Y. Ji, S. Lee, B. Cho, S. Song, and T. Lee, ACS Nano **5**, 5995 (2011).
[10]S. C. B. Mannsfeld, B. C.-K. Tee, R. M. Stoltenberg, C. V. H.-H. Chen, S. Barman, B. V. O. Muir, A. N. Sokolov, C. Reese, and Z. Bao, Nature Mater. **9**, 859 (2010).
[11]S. Lee, J.-S. Yeo, Y. Ji, C. Cho, D.-Y. Kim, S.-I. Na, B. Lee, and T. Lee, Nanotechnology **23**, 344013 (2012).
[12]H. Yan, Z. Chen, Y. Zheng, C. Newman, J. R. Quinn, F. Dotz, M. Kastler, and A. Facchetti, Nature **457**, 679 (2009).
[13]D. Khim, K. Baeg, B. Yu, S. Kang, M. Kang, Z. Chen, A. Facchetti, D. Kim, and Y.-Y. Noh, J. Mater. Chem. C **1**, 1500 (2013).
[14]S. Song, B. Cho, T.-W. Kim, Y. Ji, M. Jo, G. Wang, M. Choe, Y. Kahng, H. Hwang, and T. Lee, Adv. Mater. **22**, 5048 (2010).
[15]M. Jung, J. Kim, J. Noh, N. Lim, C. Lim, G. Lee, J. Kim, H. Kang, K. Jung, A. D. Leonard, J. M. Tour, and G. Cho, IEEE Trans. Electron Devices **57**, 571 (2010).
[16]F. C. Krebs, Org. Electron. **10**, 761 (2009).
[17]S. Lee, M. Choi, S. Han, D. Choo, J. Jang, and S. Kwon, Org. Electron. **9**, 721 (2008).
[18]A. A. Zakhidov, J.-K. Lee, J. A. DeFranco, H. H. Fong, P. G. Taylor, M. Chatzichristidi, C. K. Ober, and G. G. Malliaras, Chem. Sci. **2**, 1178 (2011).
[19]J.-K. Lee, M. Chatzichristidi, A. A. Zakhidov, P. G. Taylor, J. A. DeFranco, H. S. Hwang, H. H. Fong, A. B. Holmes, G. G. Malliaras, and C. K. Ober, J. Am. Chem. Soc. **130**, 11564 (2008).
[20]A. A. Zakhidov, H. Fong, J. A. DeFranco, J.-K. Lee, P. G. Taylor, C. K. Ober, G. G. Malliaras, M. He, and M. G. Kane, Appl. Phys. Lett. **99**, 183308 (2011).
[21]Y. Ji, M. Choe, B. Cho, S. Song, J. Yoon, H. Ko, and T. Lee, Nanotechnology **23**, 105202 (2012).
[22]S. Chung, J. Jeong, D. Kim, Y. Park, C. Lee, and Y. Hong, J. Display Technol. **8**, 48 (2012).
[23]R. V. Seidel, A. P. Graham, J. Kretz, B. Rajasekharan, G. S. Duesberg, M. Liebau, E. Unger, F. Kreupl, and W. Hoenlein, Nano Lett. **5**, 147 (2005).
[24]A. Chaudhry and M. J. Kumar, IEEE Trans. Device Mater. Reliab. **4**, 99 (2004).
[25]S. Schaur, P. Stadler, B. M.-Esteban, H. Neugebauer, and N. S. Sariciftci, Org. Electron. **13**, 1296 (2012).
[26]R. Schroeder, L. A. Majewski, and M. Grell, Appl. Phys. Lett. **84**, 1004 (2004).
[27]S. Lee, G. Jo, S.-J. Kang, G. Wang, M. Choe, W. Park, D.-Y. Kim, Y. H. Kahng, and T. Lee, Adv. Mater. **23**, 100 (2011).
[28]I. Valitova, M. Amato, F. Mahvash, G. Cantele, A. Maffucci, C. Santato, R. Martel, and F. Cicoira, Nanoscale **5**, 4638 (2013).
[29]X. Cheng, M. Caironi, Y.-Y. Noh, C. Newman, J. Wang, M. Lee, K. Banger, R. D. Pietro, A. Facchetti, and H. Sirringhaus, Org. Electron. **13**, 320 (2012).
[30]S. D. Wang, T. Minari, T. Miyadera, K. Tsukagoshi, and J. X. Tang, Appl. Phys. Lett. **94**, 083309 (2009).
[31]C. Kim, Y. Bonnassieux, and G. Horowitz, IEEE Trans. Electron Devices **60**, 280 (2013).
[32]G. Jo, J. Maeng, T.-W. Kim, W.-K. Hong, B.-S. Choi, and T. Lee, J. Appl. Phys. **102**, 084508 (2007).
[33]P. L. Bullejos, J. A. J. Tejada, F. M. Gomez-Campos, M. J. Deen, and O. Marinov, J. Appl. Phys. **106**, 094503 (2009).
[34]B. Stadlober, M. Zirkl, M. Beutl, and G. Leising, Appl. Phys. Lett. **86**, 242902 (2005).
[35]J. Lin, M. Weis, D. Taguchi, T. Manaka, and M. Iwamoto, Jpn. J. Appl. Phys., Part 1 **50**, 04DK01 (2011).
[36]H.-H. Fang, R. Ding, S.-Y. Lu, X.-L. Zhang, J. Feng, Q.-D. Chen, and H.-B. Sun, J. Mater. Chem. **22**, 24139 (2012).
[37]J.-H. Lee, H.-S. Shin, S.-I. Na, and H.-K. Kim, Sol. Energy Mater. Sol. Cells **109**, 192 (2013).
[38]T. Yokota, T. Nakagawa, T. Sekitani, Y. Noguchi, K. Fukuda, U. Zschieschang, H. Klauk, K. Takeuchi, M. Takamiya, T. Sakurai, and T. Someya, Appl. Phys. Lett. **98**, 193302 (2011).
[39]H. Klauk, M. Halik, U. Zschieschang, F. Eder, D. Rohde, G. Schmid, and C. Dehm, IEEE Trans. Electron Devices **52**, 618 (2005).
[40]S. D. Vusser, S. Steudel, K. Myny, J. Genoe, and P. Heremans, Appl. Phys. Lett. **88**, 162116 (2006).